Triangular Ising model with nearest- and next-nearest-neighbor couplings in a field

Xiaofeng Qian[1] and Henk W. J. Blöte[2,1]
[1]*Lorentz Institute, Leiden University, P.O. Box 9506, 2300 RA Leiden, The Netherlands*
[2]*Faculty of Applied Sciences, Delft University of Technology, P.O. Box 5046, 2600 GA Delft, The Netherlands*
(Received 12 May 2004; published 21 September 2004)

The authors study the Ising model on the triangular lattice with nearest-neighbor couplings $K_{\rm nn}$, next-nearest-neighbor couplings $K_{\rm nnn}>0$, and a magnetic field H. This work is done by means of finite-size scaling of numerical results of transfer matrix calculations, and Monte Carlo simulations. We determine the phase diagram and confirm the character of the critical manifolds. The emphasis of this work is on the antiferromagnetic case $K_{\rm nn}<0$, but we also explore the ferromagnetic regime $K_{\rm nn}\geqslant 0$ for $H=0$. For $K_{\rm nn}<0$ and $H=0$ we locate a critical phase presumably covering the whole range $-\infty<K_{\rm nn}<0$. For $K_{\rm nn}<0$, $H\neq 0$ we locate a plane of phase transitions containing a line of tricritical three-state Potts transitions. In the limit $H\to\infty$ this line leads to a tricritical model of hard hexagons with an attractive next-nearest-neighbor potential.

DOI: 10.1103/PhysRevE.70.036112 PACS number(s): 05.50.+q, 64.60.Ak, 64.60.Cn, 64.60.Fr

I. INTRODUCTION

The Ising model on the triangular lattice with nearest-neighbor couplings $K_{\rm nn}$, next-nearest-neighbor couplings $K_{\rm nnn}$, and a magnetic field H, is defined by the reduced Hamiltonian

$$\mathcal{H}/k_BT=-K_{\rm nn}\sum_{\langle {\rm nn}\rangle} s_is_j-K_{\rm nnn}\sum_{[{\rm nnn}]} s_ks_l-H\sum_m s_m, \qquad (1)$$

where $s_i=\pm 1$, and $\langle {\rm nn}\rangle$ and [nnn] indicate summations over all pairs of nearest neighbors and of next-nearest neighbors, respectively, as illustrated in Fig. 1.

This model, in particular the antiferromagnetic model ($K_{\rm nn}<0$), displays interesting behavior. For $K_{\rm nnn}=0$, $H=0$ the model has been solved exactly [1]. A ferromagnetic transition occurs at $K_{\rm nn}=\ln(3)/4$. An antiferromagnetic ($K_{\rm nn}<0$) mirror image of this transition is absent. This is related to the fact that the triangular lattice is not bipartite. However, at zero temperature, i.e., for $K_{\rm nn}\to-\infty$, the model displays a critical phase with algebraically decaying correlations [2]. This zero-temperature model can be exactly mapped on a solid-on-solid (SOS) model [3]. Under renormalization, it is assumed to map on the Gaussian model [4] and on the related Coulomb gas [5]. The coupling constant g_R of the Coulomb gas can thus be obtained exactly as $g_R=2$ so that a number of critical exponents can be calculated. The Ising temperature $T\propto -K_{\rm nn}^{-1}$ appears to be *relevant*: the critical state is destroyed for all $T>0$. Commensurate-incommensurate transitions occur when finite differences between the infinite nearest-neighbor couplings in the three lattice directions are introduced [3,4].

Next we consider the case of $H=0$ and $K_{\rm nnn}\neq 0$. The mapping on the SOS model (and we may also assume this for the Coulomb gas) is still valid for $K_{\rm nn}\to-\infty$ but, in the absence of an exact solution, g_R is no longer exactly known. It has, however, been deduced [4] that g_R is an increasing function of $K_{\rm nnn}$. The Coulomb gas analysis predicts that, for sufficiently large g_R, the Ising temperature becomes irrelevant, so that the algebraic phase extends to nonzero temperatures. This analysis also predicts that for even larger g_R a phase transition to a flat SOS phase occurs, both at zero and at nonzero temperatures.

Somewhat earlier, part of this scenario had already been described by Landau [6]. Via the lattice-gas representation of Eq. (1), he used the connection with the *XY* model in the presence of a six-state clocklike perturbation, made earlier by Domany *et al.* [7]. He could thus make use of their results [7] for this model which allow for the existence of a critical, *XY*-like phase in a nonzero range $K_{\rm nn}>0$. Furthermore, Landau [6] used the Monte Carlo method to verify the existence and nonuniversal character of this critical phase for the case of a fixed ratio $K_{\rm nnn}/K_{\rm nn}=-1$.

Another tool to study the model with nonzero next-nearest-neighbor couplings $K_{\rm nnn}$ is provided by the transfer-matrix technique. A simplification has been used in the latter approach: $K_{\rm nnn}$ was taken to be nonzero only for four out of the six next-nearest neighbors [8–10]. This leads to a substantial simplification of the transfer matrix calculations, but

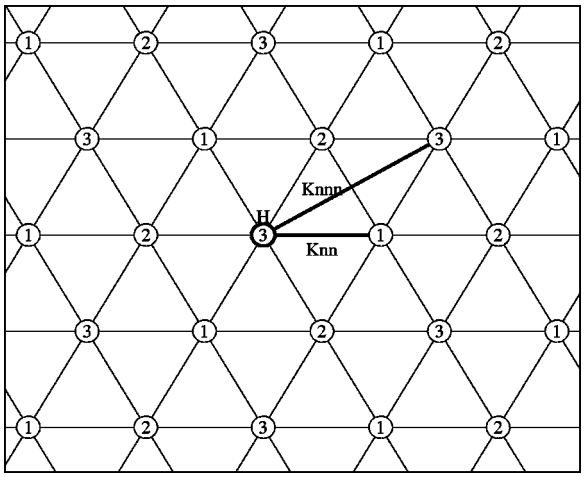

FIG. 1. The triangular lattice with nearest-neighbor couplings $K_{\rm nn}$, next-nearest-neighbor couplings $K_{\rm nnn}$ (examples of which are shown as bold bonds), and a field H (bold circle). The lattice is divided into three sublattices labeled 1, 2, and 3.

the resulting system lacks isotropy, so that applications of conformal mappings become difficult. On this basis, limited evidence [10] for the existence of the critical phase was reported; the limitation of this evidence is obviously related to the lack of sixfold symmetry.

Next we consider the consequences of a nonzero field $H>0$. On the basis of the relation with the Coulomb gas it has been derived [4] that, for $K_{\rm nn}\to-\infty$ and $K_{\rm nnn}=0$, the magnetic field H is *irrelevant*: the critical state is not destroyed by a sufficiently small field $H\neq 0$. However, the magnetic field tends to increase the Coulomb gas coupling constant g_R. The field will become marginally relevant at $g_R=9/4$ and a transition of the Kosterlitz-Thouless (KT) type or, in this context more appropriate, of the roughening type is thus expected. This transition separates the critical phase from a long-range ordered phase, where the majority of the minus-spins have condensed on one of the three sublattices of the triangular lattice. This prediction has been confirmed [11,12] by means of numerical methods. The long-range ordered phase extends to nonzero temperature $T>0$ and is separated from the disordered phase by a line of phase transitions in the (H,T) plane that belongs to the three-state Potts universality class [12–16].

Since the Ising model in a field can be mapped on a vertex model, and the critical manifolds of solvable vertex models are described by the zeroes of simple polynomials in the vertex weights [17], it may be assumed that also for the triangular lattice the critical line in the (H,T) is described by such a polynomial. This assumption was recently refuted by Qian *et al.* [12]. The shape of the critical line, as deduced from this assumption, was found to be inconsistent with the numerical evidence. They also found that the renormalization ideas originally outlined by Nienhuis *et al.* [4] could be applied to predict the shape of the critical line in the (H,T) plane for small T. This shape was found to be consistent with their numerical data for the critical line.

The aforementioned three-state Potts-type critical line is naturally part of a critical surface extending to nonzero $K_{\rm nnn}$. The more involved problem to find the phase diagram in the three-parameter (H, $K_{\rm nnn}$, $K_{\rm nn}$) space has already been partly explored. On the basis of renormalization arguments, Nienhuis *et al.* [4] obtained information about the shape of the critical surface in the limit $H\to 0$. Landau [6] performed Monte Carlo simulations for a fixed ratio $K_{\rm nnn}/K_{\rm nn}=-1$. He determined the line of phase transitions as a function of H and noted that the three-state Potts character along this line changes at a tricritical point beyond which the transition turns first order.

In this work we verify the predictions in Ref. [4] and determine the critical values of $K_{\rm nnn}$ corresponding to several relevant values of the Coulomb gas coupling constant g_R, both for finite and infinite $K_{\rm nn}$. We verify the character of the predicted critical phase at $H=0$. We also study the critical phenomena associated with the introduction of a nonzero magnetic field and explore the full three-parameter phase diagram for $K_{\rm nnn}\geqslant 0$.

This paper is organized as follows. In Sec. II, we summarize our numerical methods which include Monte Carlo algorithhms and the construction of a transfer matrix. We define the observables that will be the subject of our numerical analysis. The study of the phase transitions of the triangular Ising model with nearest- and next-nearest-neighbor couplings in a zero field is presented in Sec. III, and in Sec. IV we describe our results for a nonzero magnetic field; we conclude with a discussion in Sec. V.

II. NUMERICAL METHODS

A. Transfer-matrix calculations

Most of the the transfer-matrix calculations were performed for $T>0$ so that we had to use a binary representation for the Ising spins, leading to a transfer matrix of size $2^L\times 2^L$ for a system with finite size L. For $T=0$ one can use a simplified transfer matrix of a smaller size [11]. We define the spin lattice on the surface of a cylinder, and take the transfer direction perpendicular to a set of nearest-neighbor edges. The lattice is divided into three sublattices denoted as 1, 2, and 3, respectively, as shown in Fig. 1. Nearest-neighbor interactions occur only between different sublattices and next-nearest-neighbor interactions occur within the same sublattice.

To enable calculations for system as large as possible, a sparse matrix decomposition has been used. This leads to a very significant reduction of the required computer time and memory. The transfer matrices are defined in Refs. [11,12] for the nearest-neighbor model. Here we modify the transfer matrix to include all next-nearest-neighbor interactions. This makes it necessary to code two (instead of one) layers of spins as the transfer matrix index. Finite-size calculations with L multiples of 6 up to $L=24$ were performed. The maximum finite size $L=24$ corresponds to a cylinder with a circumference of only 12 nearest-neighbor bonds.

The magnetic correlation function along the coordinate r in the length direction of the cylinder is defined as

$$g_m(r)=\langle s_0 s_r\rangle. \tag{2}$$

At large r, this correlation function decays exponentially with a characteristic length scale ξ_m that depends on $K_{\rm nn}$, $K_{\rm nnn}$, H, and L

$$g_m(r)\propto e^{-r/\xi_m(K_{\rm nn},K_{\rm nnn},H,L)} \tag{3}$$

which can be calculated from the largest two eigenvalues λ_0 and λ_1 of the transfer matrix,

$$\xi_m^{-1}(K_{\rm nn},K_{\rm nnn},H,L)=\frac{1}{2\sqrt{3}}\ln(\lambda_0/\lambda_1), \tag{4}$$

where the factor $2\sqrt{3}$ is a geometric factor for two layers of spins. For the calculation of ξ_m, we make use of the symmetry of the eigenvectors associated with λ_0 and λ_1. The leading eigenvector (for λ_0) is invariant under a spatial inversion. In contrast, the second eigenvector is antisymmetric under inversion.

The theory of conformal invariance [18] relates ξ_m on the cylinder with the magnetic scaling dimension X_m (one-half of the magnetic correlation function exponent η). This exponent may be estimated as

$$X_m(K_{\rm nn},K_{\rm nnn},H,L) = \frac{L}{2\pi\xi_m(K_{\rm nn},K_{\rm nnn},H,L)}. \quad (5)$$

Asymptotically for a critical model with large L we have

$$X_m(K_{\rm nn},K_{\rm nnn},H,L) \simeq X_m, \quad (6)$$

where $X_m=1/(2g_R)$ in the language of Coulomb gas. This equation allows us to estimate X_m numerically and thus to obtain evidence about the universality class of the model. Or, if the universality class, and thus X_m, are considered known, Eq. (6) can be used to determine the critical surface, e.g., to solve for $K_{\rm nnn}$ for given values of $K_{\rm nn}$, H, and L. As a consequence of corrections to scaling, the solution will not precisely coincide with the critical point. The effects of an irrelevant scaling field u and a small deviation t with respect to the critical value of $K_{\rm nn}$, or $K_{\rm nnn}$, or H are expressed by

$$X_m(K_{\rm nn},K_{\rm nnn},H,L) = X_m + auL^{y_i} + btL^{y_t} + \cdots, \quad (7)$$

where a and b are unknown constants, y_i is irrelevant exponent and y_t is temperature exponent. For the solution of the equation $X_m(K_{\rm nn},K_{\rm nnn},H,L)=X_m$ we thus have $auL^{y_i}+btL^{y_t} \approx 0$, so that we expect corrections proportional to $L^{y_i-y_t}$ in the critical point estimates. For instance, for three-state Potts universality one has $y_t=6/5$ and $y_i=-4/5$ so that the leading finite-size dependence of the estimated critical points is as L^{-2}. This knowledge is helpful for the extrapolation to the actual $L=\infty$ critical point.

In addition to ξ_m, it is possible to determine a second correlation length ξ_t describing the exponential decay of the energy-energy correlation function. It is associated with a third eigenvalue λ_2 of the transfer matrix with an eigenvector that is symmetric under a spatial inversion, just as the one with eigenvalue λ_0. The pertinent eigenvalue is thus solved by means of orthogonalization with respect to the first eigenvector. In analogy with the case of the magnetic correlation length we can use the third eigenvalue λ_2 to estimate the temperaturelike scaling dimension X_t as

$$X_t(K_{\rm nn},K_{\rm nnn},H,L) = \frac{L}{2\pi\xi_t(K_{\rm nn},K_{\rm nnn},H,L)}, \quad (8)$$

where $\xi_t=(1/2\sqrt{3})\ln(\lambda_0/\lambda_2)$. At criticality, it behaves for large L as

$$X_t(K_{\rm nn},K_{\rm nnn},H,L) \simeq X_t. \quad (9)$$

Combining Eqs. (6) and (9), we can solve for two unknowns simultaneously, using the known [5] values of the tricritical three-state Potts model, namely $X_m=2/21$ and $X_t=2/7$. In this way, we can estimate the tricritical point $(K_{\rm nnn},K_{\rm nn})$ for a given H. The corrections can be argued to be proportional to $L^{y_i-y_{t2}}$ where $y_{t2}=4/7$ and $y_i=-10/7$, i.e., the corrections decay as L^{-2}.

B. Monte Carlo simulations

Since transfer-matrix calculations are, although highly accurate, restricted to small systems, we have also written Monte Carlo algorithms for the present model. To obtain good statistical accuracies we included not only a Metropolis algorithm, but also a Wolff and a geometric cluster algorithm. Which algorithm is used depends on the location in the phase diagram. The Wolff algorithm is applicable in only the case of zero magnetic field. The geometric algorithm [19] conserves the magnetization and was therefore used in combination with the Metropolis algorithm. This combination was found to work faster than the Metropolis method, but the gain in efficiency depends on the position in the three-parameter space.

Several quantities were sampled using these algorithms in order to explore the phase diagram. First we define the uniform magnetization as $m\equiv L^{-2}\Sigma_k s_k$ which tends to $\pm 1/3$ in the long-range ordered antiferromagnetic or flat phases, and to zero in the disordered (paramagnetic) phase. From its moments we define the magnetic Binder ratio as

$$Q_m = \frac{\langle m^2\rangle^2}{\langle m^4\rangle}. \quad (10)$$

Next, we consider the three-state Potts-type order parameter or, in the language of the present Ising model, the three sublattice magnetizations. We denote the magnetization density of sublattice i ($i=1$, 2, or 3) as m_i. On the basis of the staggered magnetizations we write the variance of the Potts order parameter as

$$m_s^2 = m_1^2 + m_2^2 + m_3^2 - m_1m_2 - m_2m_3 - m_3m_1 \quad (11)$$

and the corresponding dimensionless ratio as

$$Q_s = \frac{\langle m_s^2\rangle^2}{\langle m_s^4\rangle}. \quad (12)$$

At criticality, the quantities Q_m and Q_s scale as a constant plus irrelevant corrections, i.e., they converge to a constant as L increases. This property can be used for the determination of critical points.

III. NUMERICAL RESULTS FOR ZERO FIELD

We restrict this work to ferromagnetic next-nearest-neighbor interactions ($K_{\rm nnn}>0$). First, we consider the Ising model in a zero field ($H=0$), and study the phase diagram in $(K_{\rm nnn},K_{\rm nn})$ plane. We distinguish the cases $K_{\rm nn}>0$ and $K_{\rm nn}<0$.

A. Results for the ferromagnetic transition ($K_{\rm nn}>0$)

For the Ising model we have $X_m=1/8$ so that at criticality we expect that asymptotically for large L

$$X_m(K_{\rm nn},K_{\rm nnn},0,L) \simeq \tfrac{1}{8} \quad (13)$$

from which one can estimate critical points, e.g., by solving for $K_{\rm nnn}$ at a given value of $K_{\rm nn}$ or vice versa. In certain cases, critical points can be determined accurately by extrapolating to $L=\infty$. For instance, for $K_{\rm nnn}=0$ we obtain the critical value of the nearest-neighbor coupling $K_{\rm nn}=0.274\,652\,8(10)$, which is consistent with the exact result $K_{\rm nn}=\ln(3)/4$. The results are shown in Fig. 2.

We also checked that, at the decoupling point ($K_{\rm nn}=0$) the critical value of the next-nearest-neighbor coupling $K_{\rm nnn}$

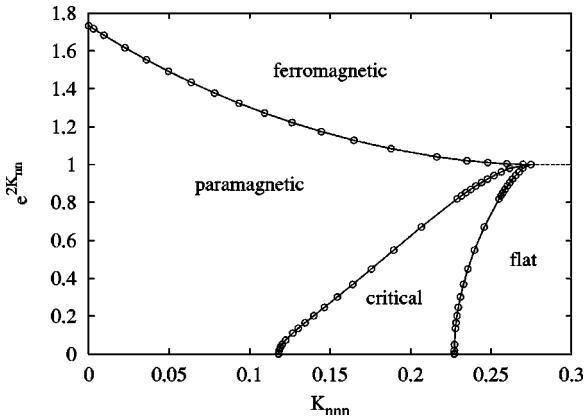

FIG. 2. Three lines of phase transitions in the ($K_{\rm nnn}$, $K_{\rm nn}$) plane. The numerically determined data points are shown as circles. The upper line displays the ferromagnetic critical line for $K_{\rm nn}>0$. For $K_{\rm nn}<0$ there are two more lines which represent the boundaries of a critical phase which resembles the low-temperature phase of the *XY* model. The two lines appear to meet at a single point, the decoupling point, at $K_{\rm nn}=0$. The right-hand critical line marks a roughening transition to a flat SOS phase, the left-hand line a KT-like transition between the disordered and the critical phases. The numerical errors in the ferromagnetic region are much smaller than the size of the symbols; for the remaining data they are difficult to estimate but believed to be at most of the same order as the symbol size.

equals the exact value $\ln(3)/4$. The three sublattices, which are also triangular lattices, become independent at the decoupling point.

B. Results for the antiferromagnetic region ($K_{\rm nn}<0$)

At finite $K_{\rm nn}<0$ and small $K_{\rm nnn}>0$, the model is obviously disordered. As described in the Introduction, with increasing $K_{\rm nnn}$ the model is expected to undergo (1) a Kosterlitz-Thouless transition to a critical phase at the point where the Coulomb gas coupling reads $g_R=4$, and the corresponding value of the magnetic dimension is $X_m=1/(2g_R)=1/8$; (2) a roughening transition to a flat phase, and the corresponding value of the magnetic dimension is thus $X_m=1/18$ at $g_R=9$. We have solved $K_{\rm nnn}$ from Eq. (6) for these two values of X_m, at several fixed values of $K_{\rm nn}$. The results were extrapolated to $L=\infty$ by means of three-point fits involving a constant (the estimated value of $K_{\rm nnn}$) plus a finite-size correction involving a free exponent. The final estimates are included in the phase diagram, Fig. 2. They suggest that the two boundaries of the critical phase merge at the decoupling point $K_{\rm nn}=0$. Our numerical results include a few special points at zero temperature ($K_{\rm nn}\to-\infty$). In the renormalization scenario, their meaning is as follows:

(1) For $g_R=9/4$ we obtain $K_{\rm nnn}=0.0185(4)$. This is where the line of roughening transitions in the ($K_{\rm nnn}$,H) plane meets the $K_{\rm nnn}$ axis.

(2) For $g_R=3$ we obtain $K_{\rm nnn}=0.0667(2)$. This is where the line of three-state Potts transitions in the plane perpendicular to the $K_{\rm nnn}$ axis comes in as a straight line with a nonzero, finite slope as argued in Ref. [12].

(3) For $g_R=4$ we obtain $K_{\rm nnn}=0.1179(2)$. This is where the KT-like line in the ($K_{\rm nnn}$,$K_{\rm nn}$) plane meets the $K_{\rm nnn}$ axis.

(4) For $g_R=9$ we obtain $K_{\rm nnn}=0.226(2)$. This is where the line of roughening transitions in the ($K_{\rm nnn}$,$K_{\rm nn}$) plane meets the $K_{\rm nnn}$ axis. This point corresponds with an actual phase transition on the $K_{\rm nnn}$ axis. We note that, in cases (1) and (3), the $K_{\rm nnn}$ axis meets with other lines of phase transitions. However, phase transitions do not occur at points (1) and (3) because the critical amplitudes vanish on the $K_{\rm nnn}$ axis.

C. Shape of the critical lines for small $|K_{\rm nn}|$

On the basis of an argument due to van Leeuwen [20], the scaling behavior of $K_{\rm nn}$ near the decoupling point ($K_{\rm nnn}=\ln(3)/4$, $K_{\rm nn}=0$), is governed by a new critical exponent $y_a=7/4$. This exponent thus determines the shape of the critical lines for small $|K_{\rm nn}|$ according to

$$K_{\rm nn}\propto\left(\frac{\ln 3}{4}-K_{\rm nnn}\right)^{7/4}. \tag{14}$$

One can find the critical exponent y_a exactly from the known properties of the magnetic correlation function of the critical Ising model. The spin-spin correlation behaves as

$$g_m(r)\propto r^{-2X_m},$$

where $X_m=1/8$ for the 2D Ising model. This also applies to the decoupling point where the model decomposes in three independent sublattices. This determines the scaling behavior of a four-spin correlation function involving spins in different sublattices in the limit of $K_{\rm nnn}\to 0$

$$g_a(r)=\langle s_{00}s_{01}s_{r0}s_{r1}\rangle=[g_m(r)]^2\propto r^{-4X_m}, \tag{15}$$

where s_{00} and s_{01} are nearest-neighbor spins belonging to different sublattices, say sublattices 1 and 2. The same applies to the pair (s_{r0}, s_{r1}) at a distance r. Equation (15) describes the energy-energy correlation associated with $K_{\rm nn}$. Its power-law decay is thus expressed by

$$g_a(r)\propto r^{-2X_a}, \tag{16}$$

where X_a is the scaling dimension of the nearest-neighbor energy density. Comparing Eq. (15) and Eq. (16), we conclude that $X_a=2X_m=1/4$ and $y_a=7/4$.

We verify Eq. (14) by plotting $K_{\rm nn}$ versus $[\ln(3)/4-K_{\rm nnn}]^{7/4}$ for the ferromagnetic critical line in Fig. 3, and for the two lines containing the algebraic phase in the antiferromagnetic region in Fig. 4. In all these cases we find approximate linear behavior near the decoupling point which confirms the predicted value of y_a.

D. The algebraic phase

The renormalization scenario predicts that, in the algebraic phase the estimates of X_m, as obtained from Eq. (5), will converge to a $K_{\rm nnn}$-dependent limit when the finite size L increases. However, in the disordered and flat phases, the system will renormalize away from the nonuniversal fixed line, and the data for X_m are therefore predicted to fan out for different values of L. We calculated X_m by solving Eq. (6) in

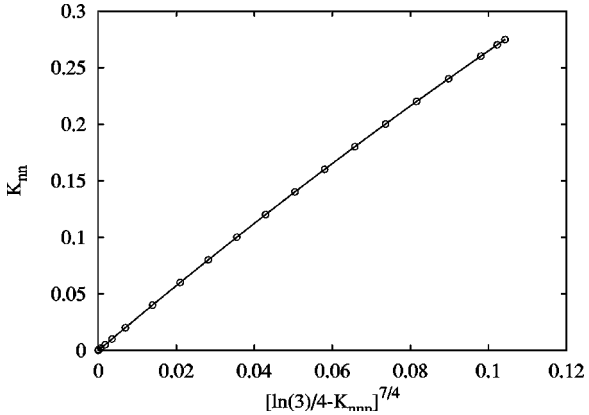

FIG. 3. The ferromagnetic critical line, plotted as $K_{\rm nn}$ versus $[\ln(3)/4-K_{\rm nnn}]^{7/4}$. The approximate linear behavior confirms that the exponent y_a associated with $K_{\rm nn}$ obeys the theoretical prediction $y_a=7/4$. The estimated errors are smaller than the symbol size.

a suitable range of $K_{\rm nnn}$ at fixed values of $K_{\rm nn}$, namely $K_{\rm nn}=-\infty$, -0.6, -0.4, -0.2, and -0.1. These results confirm the renormalization predictions, as illustrated in Figs. 5 and 6. Figure 5 shows that, for $K_{\rm nn}=-\infty$ and $H=0$, the data of X_m converge to a $K_{\rm nnn}$-dependent constant in a range of $K_{\rm nnn}$ from zero to $K_{\rm nnn}=0.226(2)$ as determined above. This confirms that for $H=0$, $K_{\rm nn}=-\infty$ the system indeed remains critical until $K_{\rm nnn}$ induces a transition to a flat phase. In contrast, Fig. 6 indicates that for nonzero temperature the critical phase starts at a positive value of $K_{\rm nnn}$. Figure 7 shows the inverse of X_m and provides a clearer picture of the transition at the large $K_{\rm nnn}$ side. We have numerically calculated the average slopes S_L of the finite-size curves in intervals specified in Table I, and fit them as follows:

$$S_L = S_\infty + aL^{y_c} + \cdots , \tag{17}$$

where S_∞ is constant, and y_c denotes the exponent of the leading finite-size correction. Results listed in Table I indicate that the finite-size dependence of the slopes is governed by a *negative* exponent y_c of L, which indicates that the slope S_L converges to a constant for $L\to\infty$, as expected in the critical range.

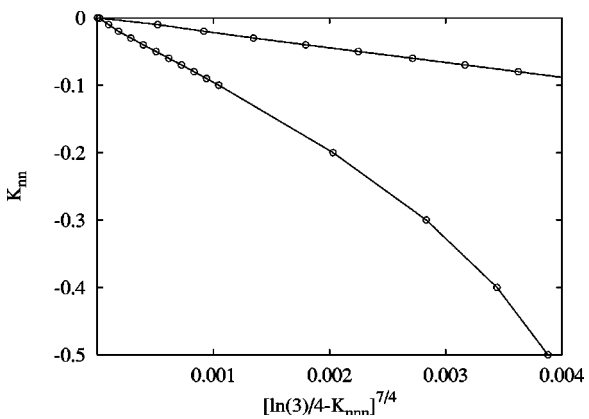

FIG. 4. Antiferromagnetic ($K_{\rm nn}<0$) critical lines near the decoupling point. The numerical results (circles) are plotted as $K_{\rm nn}$ versus $[\ln(3)/4-K_{\rm nnn}]^{7/4}$. The approximate linear behavior at small $|K_{\rm nn}|$ confirms that the exponent associated with the scaling of $K_{\rm nn}$ obeys the theoretical prediction $y_a=7/4$. The estimated errors in the data points are at most of the same order as the symbol size.

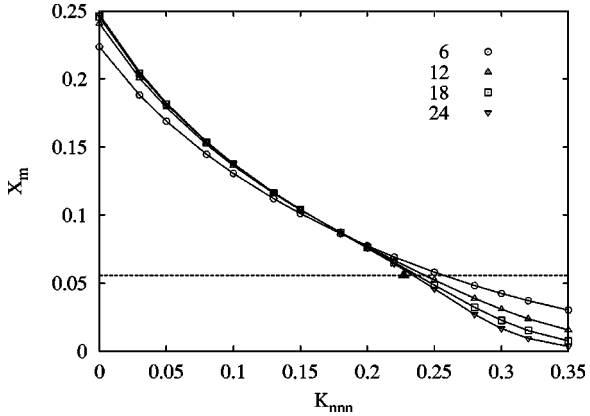

FIG. 5. Finite-size estimates of the magnetic scaling dimension X_m versus next-nearest-neighbor coupling $K_{\rm nnn}$ at $K_{\rm nn}=-\infty$. For clarity we include four lines connecting data points for system sizes $L=6$, 12, 18, 24, respectively. The dashed line indicates the special value $X_m=1/18$, and the black triangle shows the estimated critical value of $K_{\rm nnn}$ for $K_{\rm nn}\to-\infty$.

In order to provide independent confirmation of the algebraic phase, we also used the Monte Carlo method. Simulations were done for $L\times L$ systems of size $L=24$, 36, 48, and 60. Examples of the results for Q_s and Q_m are given in Figs. 8 and 9, respectively, as a function of $K_{\rm nnn}$, for $K_{\rm nn}=-0.2$. These data behave similarly as those for X_m, and show good apparent convergence to a nonuniversal, $K_{\rm nnn}$-dependent constant in the pertinent range. Note that the curves for Q_s display intersections near $K_{\rm nnn}\approx 0.207$, and those for Q_m near $K_{\rm nnn}\approx 0.245$, apparently at different sides of the algebraic phase as shown in Fig. 2. We interpret these intersections, i.e., solutions of Eq. (6) coinciding for different L, as the cancellation of the leading two L-dependent terms. Such

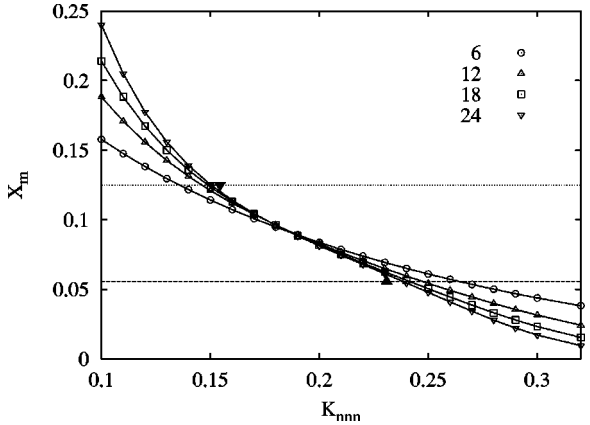

FIG. 6. Finite-size estimates of X_m versus $K_{\rm nnn}$ at $K_{\rm nn}=-0.6$. For clarity we include four lines connecting data points for system sizes $L=6$, 12, 18, 24, respectively. The dotted and dashed lines indicate the special values $X_m=1/8$ and $X_m=1/18$, respectively. The two black triangles show the estimated critical values of $K_{\rm nnn}$ at $K_{\rm nn}=-0.6$.

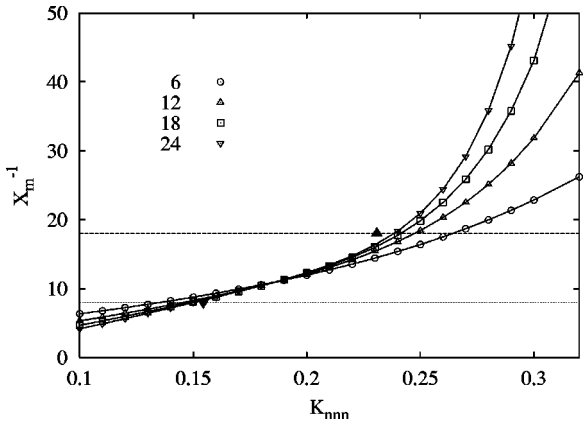

FIG. 7. Finite-size estimates of the inverse magnetic scaling dimension X_m^{-1} versus next-nearest-neighbor coupling $K_{\rm nnn}$ at $K_{\rm nn}=-0.6$. The meaning of the lines and symbols are the same as in Fig. 6. The phase transition to flat phase is clearly visible in this figure.

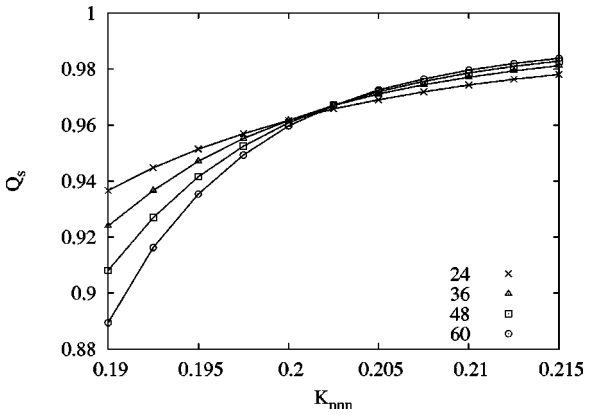

FIG. 8. Dimensionless amplitude ratio Q_s versus $K_{\rm nnn}$ at $K_{\rm nn}=-0.2$. Intersections are found to occur near the transition point between the disordered and the algebraic phases. The four lines connecting the data points represent, with increasing slope, system sizes $L=24$, 36, 48, and 60, respectively. The numerical uncertainty margins are much smaller than the size of the data points.

terms are likely associated with (1) the corrections as naturally associated with irrelevant fields in the algebraic phase; and (2) the fanning-out phenomenon mentioned above. It appears that the first types of corrections in Q_s and Q_m are of a different sign.

IV. RESULTS FOR NONZERO FIELD

In view of the Ising character of (1), we restrict ourselves to $H\geqslant 0$ without loss of generality. The phase diagram without next-nearest-neighbor interactions, i.e., in the $(H,K_{\rm nn})$ plane has already been determined by Qian *et al.* [12], with special emphasis on the limit $K_{\rm nn}\rightarrow-\infty$. In that limit, a roughening-type transition is located [11,12] near $H=0.266$. As mentioned above, the algebraic phase becomes less stable against perturbation by H when $K_{\rm nnn}$ increases, and the algebraic phase in the $(K_{\rm nnn},H)$ plane shrinks to zero at $g_R=9/4$ which corresponds, as mentioned above, to $K_{\rm nnn}=0.0185$.

The line connecting the two points $(K_{\rm nnn},H)=(0,0.266)$ and (0.0185,0) is a line of roughening transitions separating the algebraic and the ordered phases. The renormalization description implies that this line is a straight line when expressed in the scaling fields. In view of the proximity of both numerically determined points, we expect an almost straight line in the $(K_{\rm nnn},H)$ plane. The connection of the three-state Potts transition line and the roughening transition point in $(H,K_{\rm nn})$ plane has been analytically investigated by Qian *et al.* using renormalization arguments. Their analysis indicates that the roughening transition at $H=0.266$ is the end point of the Potts transition line in $(H,K_{\rm nn})$ plane for $T\downarrow 0$. Their result applies similarly to other points on the line of roughening transitions. We thus believe that this whole line serves as a frontier of the Potts critical surface, as well as the part of the $K_{\rm nnn}$ axis with g_R between $9/4$ and 4 as determined in Sec. III A.

Since three-state Potts universality implies $X_m=2/15$ at criticality, we expect that asymptotically for large L,

TABLE I. Fitted results for the extrapolated average slope $S_\infty\approx {\rm d}X_m/{\rm d}K_{\rm nnn}$ in the algebraic phase. The last column shows the exponent y_c of finite-size correction. The increase of $|S_\infty|$ with $K_{\rm nnn}$ corresponds with the narrowing of the algebraic phase when the decoupling point $K_{\rm nn}=0$ is approached. The intervals of $K_{\rm nnn}$ in which the average slopes are calculated are listed in the second column.

$K_{\rm nn}$	$K_{\rm nnn}$	S_∞	y_c
$-\infty$	0.18–0.20	−0.59 (3)	−1.1 (2)
−0.6	0.18–0.20	−0.78 (2)	−1.2 (2)
−0.4	0.18–0.22	−1.20 (8)	−0.7 (2)
−0.2	0.21–0.22	−3.3 (5)	−0.3 (1)
−0.1	0.23–0.25	−5.0 (10)	−0.2 (1)

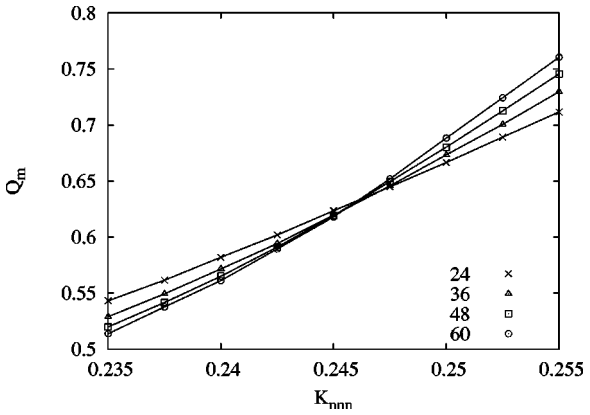

FIG. 9. Dimensionless amplitude ratio Q_m versus $K_{\rm nnn}$ at $K_{\rm nn}=-0.2$. Intersections are found to occur near the transition point between the algebraic and the flat SOS phases. The four lines connecting the data points represent, with increasing slope, system sizes $L=24$, 36, 48, and 60, respectively. The numerical uncertainty margins are much smaller than the size of the data points.

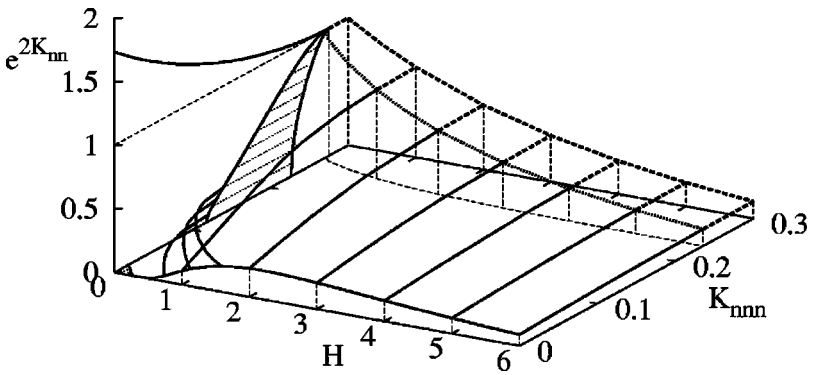

FIG. 10. The complete phase diagram in the three-parameter space $(H, K_{nnn}, e^{2K_{nn}})$. The solid lines denote second-order phase transitions, and the heavy dotted line is the tricritical line separating the three-state Potts critical sheet from the first-order sheet which is shown by heavy dashed lines. The three-state Potts critical surface is believed to connect to the $e^{2K_{nn}}=0$ plane at the KT line near the origin, and at the K_{nnn} axis until the appearance of the critical phase. The algebraic phases for $H=0$ and for $T=0$ are lightly shaded, and the thin dashed lines are projection lines added for clarity. The error margins are at most of the same order as the thickness of the lines.

$$X_m(K_{nn},K_{nnn},H,L) \simeq \tfrac{2}{15} \tag{18}$$

from which one can estimate critical points by solving for one of the three variables (K_{nn},K_{nnn},H) for specified values of the other two, and subsequent extrapolation to $L=\infty$. We thus calculated critical points on several lines at fixed values of H. The results are shown as lines connecting these points in Fig. 10. In order to zoom in on the connection of the three-state Potts transition surface and the transition lines in the (K_{nnn},K_{nn}) plane, we have also estimated critical values of H at fixed values of K_{nn}, for a suitably chosen range of K_{nnn}. Results for $K_{nn}=-0.8,-0.1,-0.15$ are included in Fig. 10. They fit well with the qualitative predictions for the shape of the critical surface [4] for small H. Furthermore, our data for the critical points at $K_{nnn}=0.0667$, corresponding with $g_r=3$, agree with the linear behavior as mentioned in Sec. III A.

Our results confirm that, when the next-nearest-neighbor coupling K_{nnn} becomes sufficiently strong, the transition from the disordered phase to the ordered phase changes character at a tricritical line, beyond which the transition turns first order. We have located the tricritical line using transfer-matrix calculations. By solving Eqs. (6) and (9) simultaneously for K_{nn} and K_{nnn} at specified values of H, we obtain results shown in Table II, and included in Fig. 10. In comparison with transfer-matrix calculations involving only X_m, the memory requirements are somewhat larger. As a consequence only three values of L up to 18 could be used. But we found that finite-size corrections are relatively small, and we are confident that the tricritical line is well determined.

TABLE II. Tricritical points as obtained by the transfer matrix method for several values of H. The decoupling point $K_{nn}=0$ is included here as the end point of the tricritical line, although it does itself not belong to the tricritical three-state Potts universality class.

H	K_{nn}	K_{nnn}
0.00	0.0000 (0)	ln(3)/4 (0)
0.05	−0.0107 (12)	0.269 (1)
0.10	−0.0214 (10)	0.2654 (5)
0.5	−0.0937 (5)	0.2572 (5)
1.0	−0.1799 (2)	0.2500 (2)
1.5	−0.2644 (2)	0.2452 (2)
2.0	−0.3481 (2)	0.2421 (2)
3.0	−0.5150 (1)	0.23845(8)
4.0	−0.6816 (1)	0.23678(8)
5.0	−0.84823 (5)	0.23599(8)
6.0	−1.01487 (5)	0.23560(8)

For sufficiently large fields H, triangles may contain at most one minus-spin and the tricritical line approaches a tricritical lattice-gas limit. In this limit the nearest-neighbor coupling and the field satisfy a linear relation

$$K_{nn} = -\frac{H}{6} + C. \tag{19}$$

As illustrated in Fig. 11, the numerical data fit this expression well, except at small H. In order to obtain a satisfactory fit to the numerical data for $H \geqslant 1$, we added terms proportional to $e^{-2H/3}$ and $e^{-4H/3}$ to Eq. (19). This fit yielded $C=-0.014\,81(5)$. A similar fit without a term proportional to H yielded $K_{nnn}=0.235\,14(7)$ for the tricritical lattice gas limit.

We have used Monte Carlo simulations to determine the location of the sheet of first-order transitions at $K_{nnn}=0.3$. We found that, depending on K_{nn} and H, a randomly initialized system evolved to a phase either largely magnetized, or resembling one of the three ordered Potts states. The threshold

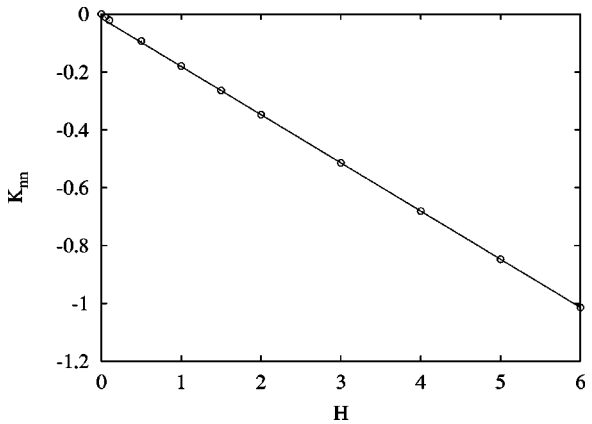

FIG. 11. The tricritical line shown as K_{nn} versus H. The numerically determined tricritical points are shown as circles, and the solid line represents the tricritical lattice-gas limit as $K_{nn}=-H/6-0.014\,81$.

values between these two regimes are shown by the heavy dashed lines in Fig. 10. They fit smoothly with the results obtained in the critical range and for the tricritical line.

V. DISCUSSION

We have determined the phase diagram of the model Eq. (1) for $K_{\rm nnn} \geqslant 0$. We locate a surface of phase transitions. This surface divides into a three-state Potts-type critical sheet and a first-order part. The two parts are separated by a tricritical line. While the determination of tricritical line becomes less accurate for small $|K_{\rm nn}|$, our data suggest that it spans the whole range $-\infty < K_{\rm nn} < 0$. This is in agreement with the minimal renormalization scenario in which the tricritical line is a flow line leading directly from the decoupling point to the tricritical fixed point.

For $H \to \infty$, minus-spins are excluded on nearest-neighbor sites and the the substitution $\sigma_i = (1 - s_i)/2$ reduces the model to a hard-hexagon lattice gas described by the reduced Hamiltonian

$$\mathcal{H}_{hh}/k_B T = V_{\rm nn} \sum_{\langle {\rm nn} \rangle} \sigma_i \sigma_j + V_{\rm nnn} \sum_{[{\rm nnn}]} \sigma_k \sigma_l - \mu \sum_m \sigma_m, \quad (20)$$

where the site variables assume values $\sigma_i = 0$, 1 and $V_{\rm nn} \to \infty$ so that nearest-neighbor exclusion applies. The chemical potential of the lattice-gas particles depends on the Ising parameters as $\mu = -12K_{\rm nn} - 12K_{\rm nnn} - 2H$, and the next-nearest-neighbor potential as $V_{\rm nnn} = -4K_{\rm nnn}$. For $V_{\rm nnn} = 0$ this model reduces to Baxter's hard-hexagon lattice gas [21]. According to the analysis presented in Sec. IV, the tricritical line persists in the lattice-gas limit. The Ising parameters C and $K_{\rm nnn}$ determine the tricritical parameters of the lattice gas as $\mu = -2.644(1)$ and $V_{\rm nnn} = -0.9406(3)$. Our findings may be compared with those of Verberkmoes and Nienhuis [22] for a model with $V_{\rm nnn} = 0$ but including additional smaller hexagons. They also report a tricritical point, attributed to an effective attraction between the hard hexagons, induced by entropic effects associated with the small hexagons.

An Ising-type tricritical point is known to occur also in the analogous case of the hard-square lattice gas [21,23,24]. Our result thus confirms that tricriticality is a generic property of hard-core lattice gases with attractive next-nearest-neighbor interactions.

Since we do not doubt the universality class of the tricritical line, we have not explicitly determined its critical exponents. However, we remark that the fast apparent convergence of the estimated tricritical points confirms that the values of the Potts tricritical exponents X_m and X_t, as used to solve Eqs. (6) and (9), do indeed apply.

Renormalization analysis predicts that the uniform magnetic field H is relevant, except for a small range $2 \leqslant g_R \leqslant 9/4$. Thus the plane $H = 0$ qualifies as a possible locus of new universality classes, in line with the existence of a critical phase such as predicted by the renormalization scenario and confirmed numerically. We finally note that the renormalization equations for the KT transitions imply that the line of KT transitions, as shown in Fig. 2 on the left-hand boundary of the critical phase, should come in as a straight line on the horizontal axis, in contrast with the numerical results which display a small part with a sudden curvature. We believe that this is a finite-size effect, explained by the same renormalization equations, which involve the marginally irrelevant temperature field parametrizing the line of KT transitions. This scaling field generates slowly converging finite-size corrections. This field and its associated finite-size effects vanish at $K_{\rm nn} = -\infty$.

ACKNOWLEDGMENTS

We are indebted to Jouke R. Heringa for his contribution to the development of the geometric cluster algorithm used in this work, and to Bernard Nienhuis for valuable discussions.

[1] R.M.F. Houtappel, Physica (Amsterdam) **16**, 425 (1950).
[2] J. Stephenson, J. Math. Phys. **11**, 413 (1970).
[3] H.W.J. Blöte and H.J. Hilhorst, J. Phys. A **15**, L631 (1982).
[4] B. Nienhuis, H.J. Hilhorst, and H.W.J. Blöte, J. Phys. A **17**, 3559 (1984).
[5] B. Nienhuis, in *Phase Transitions and Critical Phenomena*, edited by C. Domb and J.L. Lebowitz (Academic, London, 1987), Vol. 11.
[6] D.P. Landau, Phys. Rev. B **27**, 5604 (1983).
[7] E. Domany, M. Schick, J.S. Walker, and R.B. Griffiths, Phys. Rev. B **18**, 2209 (1978).
[8] H. Kitatani and T. Oguchi, J. Phys. Soc. Jpn. **57**, 1344 (1988).
[9] S. Miyashita, H. Kitatani, and Y. Kanada, J. Phys. Soc. Jpn. **60**, 1523 (1991).
[10] S.L.A. de Queiroz and E. Domany, Phys. Rev. E **52**, 4768 (1995).
[11] H.W.J. Blöte and M. P. Nightingale, Phys. Rev. B **47**, 15046 (1993).
[12] X. Qian, M. Wegewijs, and H.W.J. Blöte, Phys. Rev. E **69**, 036127 (2004).
[13] S. Alexander, Phys. Lett. **54A**, 353 (1975).
[14] W. Kinzel and M. Schick, Phys. Rev. B **23**, 3435 (1981).
[15] J.D. Noh and D. Kim, Int. J. Mod. Phys. B **6**, 2913 (1992).
[16] M.N. Tamashiro and S.R. Salinas, Phys. Rev. B **56**, 8241 (1997).
[17] F.Y. Wu, J. Math. Phys. **15**, 687 (1974).
[18] J.L. Cardy, J. Phys. A **17**, L358 (1984).
[19] J.R. Heringa and H.W.J. Blöte, Phys. Rev. E **57**, 4976 (1998).
[20] J.M.J. van Leeuwen, Phys. Rev. Lett. **34**, 1056 (1975).
[21] R.J. Baxter, J. Phys. A **13**, L61 (1980).
[22] A. Verberkmoes and B. Nienhuis, Phys. Rev. E **60**, 2501 (1999).
[23] R.J. Baxter, *Exactly Solved Models in Statistical Mechanics* (Academic, London, 1982).
[24] D.A. Huse, J. Phys. A **16**, 4357 (1983).